

## Control of Ultra- and Subharmonic Resonances

M. M. Fyrillas<sup>1</sup> and A. J. Szeri<sup>2</sup>

<sup>1</sup> University of Cyprus, Department of Mathematics and Statistics, P.O. Box 537, 1678, Nicosia, Cyprus

<sup>2</sup> University of California, Berkeley, Department of Mechanical Engineering, Berkeley, CA 94720-1740, USA

Received September 13, 1996; revised manuscript received May 21, 1997, and accepted June 20, 1997

Communicated by I. Kevrekidis

**Summary.** Periodically forced, nonlinear oscillators often show a strong response when driven near a rational multiple of the natural frequency of the linearized system: Such occurrences are known as subharmonic, ultraharmonic, and ultrasubharmonic resonances. In these systems, at these resonances, nonlinearities conspire to shift the response from the driving frequency to (near) the natural frequency of the linearized system. We demonstrate that such resonances are particularly sensitive to a very slight modulation of the forcing to include a component at (near) the natural frequency. This modulation can be constructed—using techniques developed herein—to annihilate or to enhance the subharmonic or ultraharmonic resonance. The ideas are first introduced using a multiple-scales perturbation analysis of the Duffing equation. Later, fully nonlinear techniques are developed that can be implemented using continuation algorithms on a computer. For example, optimal control theory is used to devise a very small modulation of the forcing that annihilates the principal subharmonic of the Duffing equation via a contrived saddle-node bifurcation of periodic orbits. Following this manufactured saddle-node bifurcation, the surviving attractor is of a much smaller amplitude. Similar efforts aimed at the sharp ultraharmonics of the Rayleigh-Plesset equation of nonlinear bubble dynamics are equally successful—although the rich modal structure of the response requires some variations on the control strategy. Finally, these ideas open up the possibility of controlling the shape of broad areas of the response diagrams important in many applications.

### 1. Introduction

Driven nonlinear oscillators often have a large response when the forcing frequency and the natural frequency are related by an integer (or nearly so). The classical book by Hayashi [11] is a careful exposition of many such resonances. These resonances are ubiquitous in many systems: for example, in the nonlinear oscillations of a bubble driven

by an acoustic field. The work of Lauterborn [16], [21] on response diagrams of driven bubbles shows a great many resonances crowding together at larger amplitudes of the forcing.

### ***1.1. Controlling Resonances***

Such resonances can be problematic. For example, in medical imaging using ultrasound (and in therapeutic ultrasound), bubbles may be induced to grow by the process of rectified diffusion [5], [10]. These bubbles can have disastrous consequences for a patient. The bubble growth is fastest when bubbles are driven at or near one of these resonances. An important limitation on one's ability to control a bubble oscillation is that it is impossible to attach actuators to the bubble to effect some desired control. Similarly, it is not feasible to alter physical parameters such as the surface tension on the bubble interface to change the dynamics in some desired way. The only practical way in which one can control the bubble dynamics is by alteration of the forcing—which means changing the amplitude, the phase, or the waveform of the acoustic forcing. If we assume that one wants to alter the driving as little as possible (it may be optimal for resolving some structure), this presents a difficult problem.

Resonances are of importance in the acoustic response of bubble clouds. Yoon et al. [36] demonstrated that the bubbles in bubble clouds oscillate collectively (in a synchronized fashion) at resonant frequencies far lower than the frequencies of individual bubbles. Kumar and Brennen [15] observed 'harmonic cascading' in their clever experiments on bubble clouds bounded by an oscillating wall. Harmonic cascading is an example of an ultraharmonic resonance. Prosperetti et al. [22] and Sarkar and Prosperetti [24] examined the resonances and acoustic backscatter from bubble clouds at the sea surface. These resonances of bubbly liquids can have important ramifications in turbomachinery [6].

Control techniques have been applied to some similar acoustic emission problems by Pan et al. [20]. These authors report successful far-field acoustic control of sound generated by oscillations of a rectangular panel. These radiated sounds are associated with resonant shape oscillations of the panel, which is driven either by structural vibration or by an exciting incident sound field. Control is achieved by designing the controlling sound field so as to reduce modal amplitudes of vibration of the panel.

### ***1.2. Enhancing Resonances***

An alternative challenge is involved in enhancing a resonance. Resonances are at the basis of a large array of detection and physical characterization strategies. In many cases, it is advantageous to enhance a resonance so as to improve chances of detection of some structure against a field of background noise. This is an issue, for example, in *in vivo* bubble detection [2], [23] in medical applications, and in the detection of transient cavitation [2].

Several types of nondestructive testing are based on resonances. For example, in [13], [14] noncontact simultaneous electromagnetic excitation and detection of ultrasonic waves is used to probe grain size, bonding, and delamination in thin sheets of conducting

materials. The importance of resonance in this context is to raise the signal-to-noise ratio to detectable levels.

Finally, it has been shown that subharmonic modes of free shear flows are effective in controlling the development of these flows. It was first shown by Ho and Huang [12] that subharmonic forcing dramatically increases the spreading rate of a shear layer. Chen et al. [4] have shown the importance of phase differences between the subharmonic and the fundamental mode in the control problem for compressible wakes. Maekawa and Mansour [18] confirm similar phenomena through numerical simulations of a plane wake.

### 1.3. Plan of the Paper

In developing the subject, we shall focus on two equations: the Duffing equation and the Rayleigh-Plesset equation of nonlinear bubble dynamics. The Duffing equation is an attractive subject of study, because good approximations to its ultra- and subharmonic resonances may be developed by the method of multiple scales. The incarnation of the Duffing equation of interest in this paper is

$$\frac{d^2x}{dt^2} + \alpha x + \epsilon x^3 + \epsilon k \frac{dx}{dt} = \Gamma \cos(\omega t) + \tilde{F}(t). \quad (1)$$

For small  $\epsilon$ , the system is weakly damped and weakly nonlinear. The forcing  $\Gamma \cos(\omega t)$  drives the main resonance when  $\omega \approx \sqrt{\alpha}$ . We take the modulation  $\tilde{F}(t)$  to be zero for the time being. The 1/3 (principal) subharmonic occurs when the forcing  $\Gamma \cos(\omega t)$  is near three times the natural frequency, i.e., when  $\omega \approx 3\sqrt{\alpha}$ . The 3/1 (principal) ultraharmonic occurs when the forcing  $\Gamma \cos(\omega t)$  is one-third the natural frequency, i.e., when  $\omega \approx \sqrt{\alpha}/3$ . We will show that these resonances may be annihilated or enhanced by very small modulations (controls)  $\tilde{F}(t)$ .

The Rayleigh-Plesset equation is also a second-order forced, damped nonlinear oscillator. It is worthy of study because it displays large-scale, sharp ultraharmonic resonances. Moreover, unlike the Duffing resonances, the Rayleigh-Plesset resonances feature rich contributions by many, many modes to the response. As such, Rayleigh-Plesset resonances present some interesting challenges, as we shall see.

In what follows, we shall first review the structure of the principal subharmonic and principal ultraharmonic of the Duffing equation using the method of multiple scales. We will show how effectively a very small modulation of the forcing by an additional component at the main harmonic can alter the phase portrait of the system for the slowly varying amplitudes of the harmonic response. The special ability to alter the phase portrait of an ultra- or subharmonic resonance is the basis of the control strategies we develop in the sections that follow. Finally we consider the related problem of controlling whole regions of the response diagram.

## 2. Related Work

The subject of resonant responses of forced, damped ordinary differential equations is a vast one. We shall mention recent work on the control of bifurcation points, on optimal forcing, and on the control of chaos.

In several papers, Abed and coworkers [1], [32] demonstrated that it is possible to construct a feedback control of an ODE that undergoes a bifurcation from a steady solution, so as to move the bifurcation point. In one instance [32], this allowed the authors to prevent the onset of chaotic motions, which arose from homoclinic bifurcation of a periodic orbit born in a subcritical Hopf bifurcation. By delaying the subcritical Hopf bifurcation to higher values of the bifurcation parameter, the onset of chaotic dynamics was also delayed. This is possible using linear feedback. It was further demonstrated that the subcritical Hopf bifurcation could be rendered supercritical using a nonlinear feedback control. They applied their theory to a thermal convection loop model, showing that chaotic behavior was replaced by either a convective equilibrium or a small amplitude limit cycle. These ideas were tested in experiments on a thermal convection loop by Yuen and Bau [37].

Doedel et al. [7] discussed the control of limit points and Hopf bifurcation points (both of equilibria) by optimization. Another problem of interest to them was the control of the distance between two limit points (of equilibria) so as to eliminate hysteresis. Later, in infinite dimensions, Doedel et al. [8] developed numerical techniques for the optimization of objective functions that depend on variable solutions of ODEs. As examples, they optimized the location of a limit point of solutions to a boundary value problem. In a second example, they optimized a scalar objective function with respect to the choice of three scalar parameters in a boundary value problem.

There has been considerable interest in period-doubling bifurcations and their control—due, in part, to important applications in parametric amplifiers based on the Josephson effect. Wiesenfeld and McNamara [34], [35] noted that at a value of a control parameter just before a supercritical period-doubling bifurcation, certain systems acted as amplifiers of white noise. The response was characterized by broadband peaks in the power spectrum, centered about the new frequencies that arise in the (incipient) period-doubling bifurcation. This led the authors to try perturbing the system with a periodic signal, with frequency equal to that of the (incipient) period-doubled response ( $\omega/2$ ). It was found that the signal was dramatically amplified at frequency  $\omega$ . This conclusion was based on analysis of a disturbance evolution equation linearized about the orbit which is about to period-double. Wiesenfeld and McNamara also reported analog simulations of the Duffing equation forced by two frequencies. In a later paper, Bryant and Wiesenfeld [3] developed a nonlinear disturbance evolution equation loosely analogous to a normal form. Analysis of this normal form suggested that the period-doubling bifurcation point was moved by the perturbing signal, by an amount proportional to the amplitude of the signal to the  $2/3$  power. They also showed similar amplification effects for other codimension 1 bifurcations of periodic orbits: saddle-node and transcritical, pitchfork, and Hopf.

Subsequently, in several papers Svensmark and collaborators [26], [27], [28] demonstrated the importance of the presence of perturbing noise in addition to the signal. They also reported the results of experiments on Josephson tunnel junctions that showed the effect. Finally, they advanced an alternative “normal form” for the perturbed period-doubling bifurcation; however, this was later shown to give incorrect behavior by Vohra and Wiesenfeld [31].

A last contribution of interest in this area by Vohra, Fabiny, and Wiesenfeld [30] showed that a subcritical period-doubling bifurcation can be destabilized by a small

periodic signal at the period-doubled frequency. This was demonstrated experimentally using a driven magnetostrictive oscillator. Interestingly, the experiment showed that in a case where there was hysteresis, with the subcritical period-doubling followed soon after by a limit point on the same branch, the perturbation affected the response diagram unevenly. Although the perturbation was effective at moving the subcritical period-doubling bifurcation point to the left (destabilizing), the limit point was essentially unchanged. Vohra and Wiesenfeld [31] attribute this to nonresonant forcing at the limit point.

There have been interesting developments in variational calculus related to techniques we pursue in the present work. Wargitsch and Hübler [33] examined the optimal forcing of damped ODEs, where the goal was to achieve the maximum energy of the response by a certain time, starting from a given initial condition. These authors found that the solution to the optimal control problem was provided by the time-reversed dynamics of the unforced problem.

Earlier, we alluded to prevention of chaotic dynamics. There are a number of papers that concern the control of otherwise chaotic orbits. The goal is to force a chaotic trajectory to follow an unstable periodic orbit by stabilizing it with a periodic perturbation of parameter(s) in the system. This is an open-loop alternative to schemes based on the feedback method proposed by Ott, Grebogi, and Yorke [19]. For a recent review of research in this area, one may consult Shinbrot [25].

### 3. Multiple-Scales Analysis of the Principal Resonances of the Duffing Equation

Now we turn to a motivation of our control schemes using the method of multiple scales. It is convenient to recast (1) in dimensionless time; hence, we set  $\tau = \omega t/\eta$ . The value of  $\eta$  corresponds to the order of the resonance under investigation; for example,  $\eta = 3$  yields the 1/3 (principal) subharmonic, whereas  $\eta = 1/3$  yields the 3/1 (principal) ultraharmonic. The Duffing equation then reads

$$\frac{\omega^2}{\eta^2} \frac{d^2x}{d\tau^2} + \alpha x + \epsilon x^3 + \epsilon \frac{\omega k}{\eta} \frac{dx}{d\tau} = \Gamma \cos(\eta \tau) + F(\tau). \quad (2)$$

#### 3.1. The 1/3 Subharmonic Resonance

First, we shall look for the frequency at which the subharmonic occurs. A convenient measure of detuning is  $\omega_1$  where  $\omega = 3(\omega_0 + \epsilon\omega_1)$ . Similarly, we expand  $x(\tau) = x_0(\tau) + \epsilon x_1(\tau) + \dots$ . To leading order (2) with  $\eta = 3$  becomes

$$\omega_0^2 \frac{d^2x_0}{d\tau^2} + \alpha x_0 = \Gamma \cos(3\tau). \quad (3)$$

The solution is

$$x_0(\tau) = a \cos\left(\frac{\sqrt{\alpha}}{\omega_0} \tau\right) + b \sin\left(\frac{\sqrt{\alpha}}{\omega_0} \tau\right) + x_{0,p}(\tau),$$

where  $x_{0,p}(\tau)$  is the particular solution. If we demand  $2\pi$ -periodicity of  $x_0$ , then  $\omega_0 = \sqrt{\alpha}$ .

An approximation to the subharmonic response is readily obtained by use of the method of multiple scales. This exploits the two natural time scales in the problem: (i) rapid oscillations at the natural frequency or thereabouts, and (ii) slow evolution to an attractor (when  $\epsilon$  is small) in the slow time  $T = \epsilon\tau$ . Then, by expanding the solution in the form

$$x(\tau; \epsilon) = x_0(\tau, T) + \epsilon x_1(\tau, T) + \dots,$$

we find that the leading order system is

$$\alpha \left( \frac{\partial^2 x_0}{\partial \tau^2} + x_0 \right) = \Gamma \cos(3\tau), \quad (4)$$

with solution

$$x_0(\tau, T) = a(T) \cos(\tau) + b(T) \sin(\tau) - \frac{\Gamma}{8\alpha} \cos(3\tau). \quad (5)$$

The  $T$ -dependent coefficients  $a$  and  $b$  are determined by eliminating secular behavior at the next order.

To order  $\epsilon$ , we have the system

$$\alpha \left( \frac{\partial^2 x_1}{\partial \tau^2} + x_1 \right) = (\dots) \cos(\tau) + (\dots) \sin(\tau) + \dots. \quad (6)$$

In order that the expansion remain well-ordered with respect to  $\epsilon$ , we require that the coefficients of the forcing components  $\cos(2\pi\tau)$  and  $\sin(2\pi\tau)$  on the right-hand side of (6) vanish. This leads to the following system for  $a$  and  $b$ :

$$\begin{aligned} \frac{da}{dT} &= -\frac{k a(T)}{2\sqrt{\alpha}} + \frac{3\Gamma^2 b(T)}{256\alpha^3} \\ &\quad - \frac{\omega_1 b(T)}{\sqrt{\alpha}} + \frac{3\Gamma a(T) b(T)}{32\alpha^2} + \frac{3b(T)}{8\alpha} [a(T)^2 + b(T)^2], \end{aligned} \quad (7)$$

and

$$\begin{aligned} \frac{db}{dT} &= \frac{-3\Gamma^2 a(T)}{256\alpha^3} + \frac{\omega_1 a(T)}{\sqrt{\alpha}} \\ &\quad - \frac{k b(T)}{2\sqrt{\alpha}} + \frac{3\Gamma}{64\alpha^2} [a(T)^2 - b(T)^2] - \frac{3a(T)}{8\alpha} [a(T)^2 + b(T)^2]. \end{aligned} \quad (8)$$

Equilibria in the  $a$ - $b$  system correspond to periodic orbits of (2) through (5). A typical phase portrait of the  $a$ - $b$  system is shown in Figure 1(a), where the nontrivial nodes correspond to the principal subharmonic. Note that the larger part of the subharmonic response is carried by the harmonic component with amplitude coefficients  $(a, b)$ .

Now, in the multiple-scales system we can motivate the control technique which is the central focus of this paper. In what follows, we switch on the modulation  $F(\tau) = \epsilon\gamma \cos(\tau)$  of the subharmonic drive. Some comments are in order. This additional forcing is near the main harmonic of the nonlinear oscillator (depending on the detuning). Because the period of the subharmonic drive  $\Gamma \cos(3\tau)$  is an integer multiple of the period

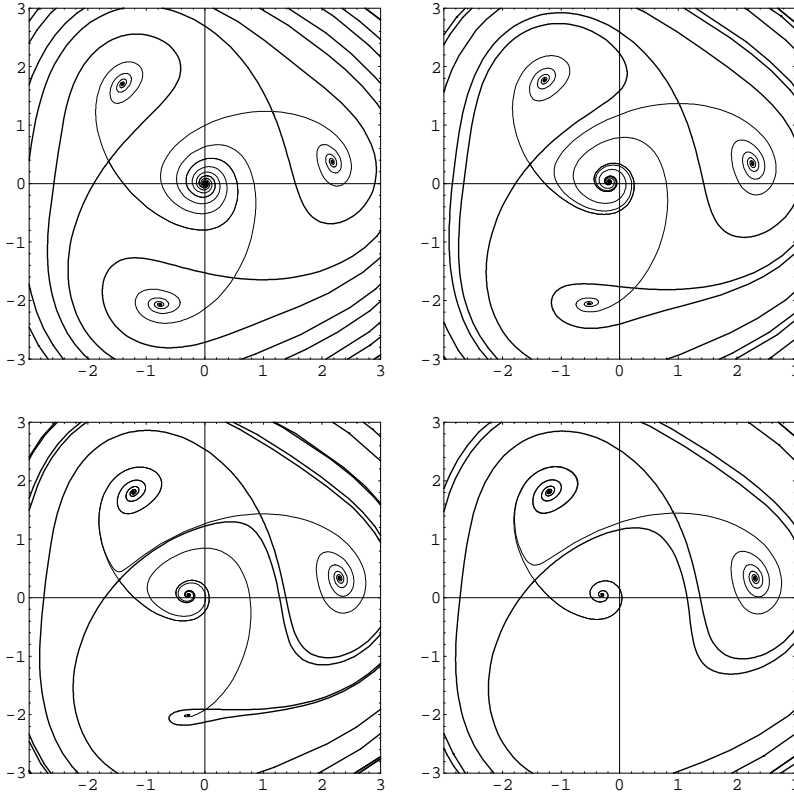


**Fig. 1.** Control of the principal subharmonic of the forced, damped Duffing equation. These are phase portraits for the slowly varying amplitudes of the harmonic components  $a(T)$  and  $b(T)$  in (5). The orbits are computed at  $\epsilon = 0.01$  with detuning  $\omega_1 = 5/3$ , damping  $k = 0.5$ , and subharmonic drive amplitude  $\Gamma = 5$ . The finer curves are the unstable manifolds of the saddles; the heavier curves are the stable manifolds. (a) Uncontrolled case. The nontrivial nodes correspond to the subharmonic (periodic) attractors. (b) Phase portrait including the modulation (control) at the main harmonic  $0.005 \cos(\tau)$ ; note the saddle and node in the third and fourth quadrants have drawn closer than in (a). (c) Amplitude of the modulation increased to  $0.0075$ . (d) At amplitude  $0.008$  of the modulation, the node and the saddle in the third and fourth quadrants have been annihilated in a saddle-node bifurcation. Note that the basin of attraction of the small amplitude node has enlarged to include those points that were attracted to the subharmonic node in (a).

of the modulation, we are not destroying the periodicity of the attractors. Finally, the multiple-scales setting continues to provide an excellent approximation for the dynamics. The system has changed slightly from (7, 8) as there is the modulation which yields additional secular terms to be eliminated—the changes to the system are straightforward to compute.

Now, we shall examine the fate of the main features of the phase portrait for the  $(a, b)$ -system as  $\gamma$  is increased from  $\gamma = 0$ ; see Figure 1. As long as the fixed points

of the  $(a, b)$ -system remain hyperbolic, they will survive under small increments of  $\gamma$ . This statement applies equally well to the underlying periodic orbits of the full system.

When  $\epsilon\gamma = 0.005$ , we see in Figure 1(b) that the saddle-node pair that inhabits the third and fourth quadrants has drawn a little closer. If we further increase the amplitude to  $\epsilon\gamma = 0.0075$ , we see the picture in Figure 1(c). The saddle-node pair in the third and fourth quadrants is very much closer. Also, there has been a global bifurcation between Figures 1(b) and 1(c): A saddle connection was formed and broken between the saddles in the first and second quadrants. This is important as the stable manifold of the saddle in the second quadrant becomes the basin boundary of the attractor that “takes over” when we have finally annihilated the saddle-node pair in Figure 1(d). Here, the modulation with amplitude  $\epsilon\gamma = 0.008$  has obliterated the original subharmonic attractor in the third quadrant of the unperturbed system in Figure 1(a).

Those points that were in the basin of attraction of the third-quadrant subharmonic in Figure 1(a) now find themselves in the basin of attraction of a much smaller amplitude orbit whose signature is a node near the origin in Figure 1(d). It is interesting to note that the other two subharmonics are largely unaffected by the control that annihilated the third-quadrant subharmonic. It is also curious that the amplitude of the modulation that annihilates the subharmonic is three orders of magnitude *smaller* than the subharmonic drive itself.

Why should one expect that the subharmonic node should be so susceptible to manipulation by such minute modulation at the main harmonic? Well, it is important to keep in mind that, although the subharmonic is driven at (roughly) three times the frequency of the main harmonic, the larger part of the response is at the main harmonic—i.e.,  $a(T)$  and  $b(T)$ . There is a smaller component of the response at the subharmonic drive frequency (see (5)), and other yet smaller components at higher multiples of the main harmonic frequency (and higher order in  $\epsilon$ ). Thus the subharmonic resonant *response* is largely harmonic and therefore especially susceptible to control at the main harmonic. We return to this point later.

### 3.2. The 3/1 Ultraharmonic Resonance

The ultraharmonic response of the Duffing equation may be similarly manipulated by a very small modulation of the driving. Again, it is possible to appreciate how this works by a multiple-scales analysis of the system

$$9\omega^2 \frac{d^2x}{d\tau^2} + \alpha x + \epsilon x^3 + 3\epsilon\omega k \frac{dx}{d\tau} = \Gamma \cos(\tau/3) + F(\tau),$$

with  $\omega = \frac{1}{3}(\sqrt{\alpha} + \epsilon\omega_1)$ . To leading order in  $\epsilon$ , the solution is

$$x_0(\tau, T) = a(T) \cos(\tau) + b(T) \sin(\tau) + \frac{9\Gamma}{8\alpha} \cos(\tau/3). \quad (9)$$

We remark that the multiple-scales analysis for the principal ultraharmonic is not quite as accurate an approximation because the resonance occurs at a larger value of the detuning [11]. In Figure 2(a) we show the phase portrait for the  $(a(T), b(T))$ -system with pure ultraharmonic drive at the parameter values  $\Gamma = 3$ ,  $\omega_1 = 15$ , and  $\kappa = 0.5$ .

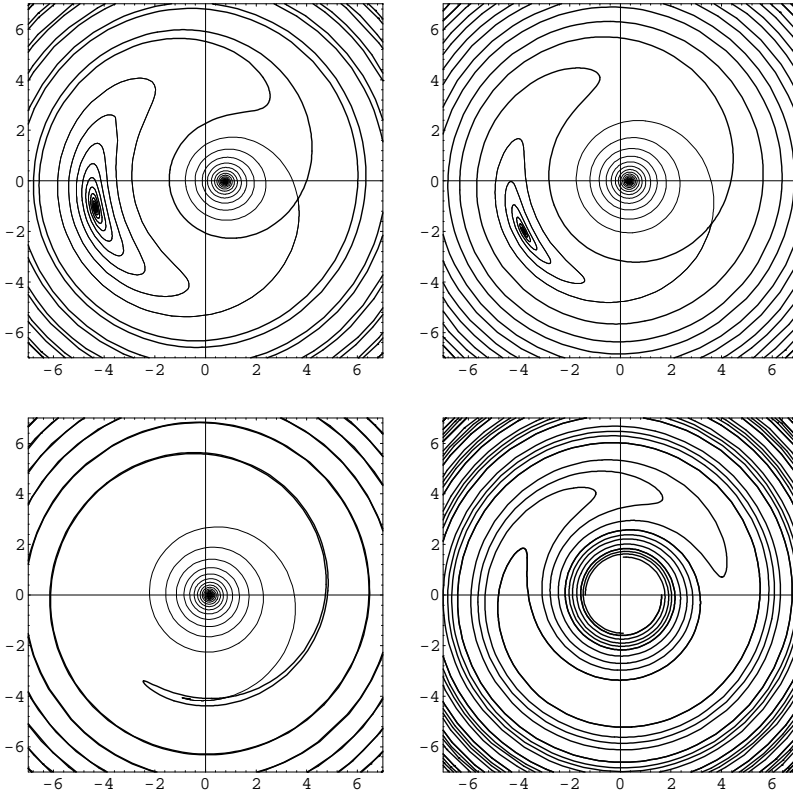


**Fig. 2.** Control of the principal ultraharmonic of the forced, damped Duffing equation. These are phase portraits for the slowly varying amplitudes of the harmonic components  $a(T)$  and  $b(T)$  in (9). The orbits are computed at  $\epsilon = 0.01$  with detuning  $\omega_1 = 15$ , damping  $k = 0.5$ , and ultraharmonic drive amplitude  $\Gamma = 3$ . In (a)–(c), the finer curves show the unstable manifolds of the saddle; the heavier curves are the stable manifolds. (a) Uncontrolled case. The larger amplitude node in the third quadrant corresponds to the ultraharmonic resonance. (b) Phase portrait including the modulation (control) at the main harmonic  $0.05 \cos(\tau)$ ; note the saddle and node in the third and fourth quadrants have drawn closer. (c) Amplitude of the modulation increased to  $0.075$ . (d) At amplitude  $0.08$  of the modulation, the node and the saddle have been annihilated in a saddle-node bifurcation. The basin of attraction of the small amplitude node has enlarged to include the whole space.

There are three fixed points for the system of slowly varying amplitudes: a node near the origin that corresponds to a small-amplitude periodic attractor, a saddle in the fourth quadrant that corresponds to a saddle periodic orbit, and finally a large-amplitude node periodic orbit in the third quadrant. The latter is the ultraharmonic resonance.

Now we watch the changes in the phase portrait as the ultraharmonic forcing is subtly modulated by mixing in  $F(\tau) = \epsilon\gamma \cos(\tau)$ . When  $\epsilon\gamma = 0.05$  we see in Figure 2(b) that the saddle and node in the third and fourth quadrants have drawn slightly closer. When  $\epsilon\gamma = 0.075$  in (c), the saddle and node are very close, and the basin of attraction of the

large-amplitude node (the ultraharmonic resonance) has shrunk dramatically. Finally, in (d), the saddle and node have been annihilated in a saddle-node bifurcation. The only attractor that remains is the node with much smaller amplitude. What caused the dramatic destruction of the ultraharmonic resonance is the modulation  $F$ —which is two orders of magnitude smaller than the ultraharmonic drive.

Thus, we observe a second time that in the presence of an ultra- or subharmonic resonance, the topology of the phase portrait can be manipulated with subtle modulation at the main harmonic. This makes it possible to annihilate the ultra- or subharmonic, leaving behind an attractor with a much smaller amplitude.

#### 4. Optimal Control

These two motivational examples based on weak nonlinearity and weak detuning are valuable as a guide for how to proceed in a fully nonlinear calculation. As a practical matter, we were able to analyze the dynamics by considering just the 2-D phase portraits for the slowly varying amplitudes of the harmonic part of the response. The topological changes we forced with  $F(\tau)$  included the removal of a simply connected region of the phase plane that corresponded to the stable manifold of a node that ceased to exist when it was destroyed in a saddle-node bifurcation. It is interesting to note that the control of the topology of the phase portrait for the slow  $\epsilon\tau$ -system was effected on the fast time scale  $\tau$ .

Now, we want to move on to consider the strongly nonlinear and hence more strongly detuned system when  $\epsilon$  is not restricted to be small. In this setting there is no convenient separation of time scales to exploit to recast the dynamics as an autonomous 2-D system for  $a(T)$  and  $b(T)$ . Instead, we must confront a more complicated geometrical structure.

In the fully nonlinear setting, it is still true that an ultra- or subharmonic attractor is born (or dies) in a saddle-node bifurcation—but now we must regard it as a saddle-node bifurcation of periodic orbits. Hence our intuition is that such an attractor might be susceptible to destruction in a saddle-node bifurcation of periodic orbits. This leads to the following idea: Why not try to accomplish this using optimal modulation of the forcing?

For simplicity we focus first on the principal subharmonic. We formulate an optimal control problem, the goal of which is to find the most efficient  $F(\tau)$  that drives the node periodic orbit (the subharmonic response) and its sister saddle periodic orbit to coalesce. This will eliminate the pair. Accompanying the elimination of the pair will be a global topological change in the system: an attractor, together with its basin of attraction, will have been eliminated. What takes over remains to be seen.

##### 4.1. Control of the 1/3 Subharmonic of the Duffing Equation

It is convenient to recast the Duffing equation (1) onto a unit time interval; hence, we set  $\tau = \omega t / (6\pi)$ . The equations satisfied by the node periodic orbit  $x(\tau)$  and by the saddle

periodic orbit  $y(\tau)$  may be written  $\mathcal{G} = 0$  and  $\mathcal{H} = 0$ , where

$$\mathcal{G}(x, x_\tau, x_{\tau\tau}, F) \equiv \frac{\omega^2}{36\pi^2} \frac{d^2x}{d\tau^2} + \alpha x + \epsilon x^3 + \epsilon \frac{\omega k}{6\pi} \frac{dx}{d\tau} - \Gamma \cos(6\pi\tau) - F(\tau), \quad (10)$$

and

$$\mathcal{H}(y, y_\tau, y_{\tau\tau}, F) \equiv \frac{\omega^2}{36\pi^2} \frac{d^2y}{d\tau^2} + \alpha y + \epsilon y^3 + \epsilon \frac{\omega k}{6\pi} \frac{dy}{d\tau} - \Gamma \cos(6\pi\tau) - F(\tau). \quad (11)$$

Note that the subscript  $\tau$  denotes differentiation with respect to time. We want to reduce to zero the difference between the two periodic orbits,

$$\int_0^1 (x(\tau) - y(\tau))^2 d\tau, \quad (12)$$

using a minimum modulation, as measured by, for example,

$$\int_0^1 F^2(\tau) d\tau.$$

To accomplish this task, we form the function

$$J = \int_0^1 [\mu(x - y)^2 + F^2 - \lambda\mathcal{G} - \phi\mathcal{H}] d\tau. \quad (13)$$

When  $\mathcal{G} = 0$  and  $\mathcal{H} = 0$ , the integral  $J$  is the cost function in our optimal control problem. The cost depends on both the difference between the node periodic orbit and the saddle periodic orbit, and on the amount of modulation required to do the job. The constant  $\mu$  can be interpreted as a weighting factor that affects how much  $\|F\|_2^2$  we are willing to tolerate to bring  $x$  and  $y$  closer. Note that we have incorporated two copies of the Duffing equation into the cost function, as these are now regarded as constraints on the functions  $x$  and  $y$ . Because these are differential constraints, there is associated with each a time-dependent Lagrange multiplier ( $\lambda(\tau)$  and  $\phi(\tau)$ , respectively).

We are interested in the case where the cost function achieves a minimum with respect to variations in the modulation. The necessary condition is that the first variation of  $J$  should be zero. The first variation is

$$\begin{aligned} \delta J = & \int_0^1 2\mu(x - y) \delta x - 2\mu(x - y) \delta y + 2F \delta F - \mathcal{G} \delta \lambda - \mathcal{H} \delta \phi \\ & - \lambda \frac{\partial \mathcal{G}}{\partial x} \delta x - \lambda \frac{\partial \mathcal{G}}{\partial x_\tau} \delta x_\tau - \lambda \frac{\partial \mathcal{G}}{\partial x_{\tau\tau}} \delta x_{\tau\tau} - \lambda \frac{\partial \mathcal{G}}{\partial F} \delta F \\ & - \phi \frac{\partial \mathcal{H}}{\partial y} \delta y - \phi \frac{\partial \mathcal{H}}{\partial y_\tau} \delta y_\tau - \phi \frac{\partial \mathcal{H}}{\partial y_{\tau\tau}} \delta y_{\tau\tau} - \phi \frac{\partial \mathcal{H}}{\partial F} \delta F d\tau. \end{aligned}$$

Next, it is useful to integrate certain terms by parts. This yields

$$\begin{aligned}
 \delta J = & \int_0^1 \left[ 2F - \lambda \frac{\partial \mathcal{G}}{\partial F} - \phi \frac{\partial \mathcal{H}}{\partial F} \right] \delta F - \mathcal{G} \delta \lambda - \mathcal{H} \delta \phi \\
 & + \left[ 2\mu(x-y) - \lambda \frac{\partial \mathcal{G}}{\partial x} + \frac{d}{d\tau} \left( \lambda \frac{\partial \mathcal{G}}{\partial x_\tau} \right) - \frac{d^2}{d\tau^2} \left( \lambda \frac{\partial \mathcal{G}}{\partial x_{\tau\tau}} \right) \right] \delta x \\
 & + \left[ -2\mu(x-y) - \phi \frac{\partial \mathcal{H}}{\partial y} + \frac{d}{d\tau} \left( \phi \frac{\partial \mathcal{H}}{\partial y_\tau} \right) - \frac{d^2}{d\tau^2} \left( \phi \frac{\partial \mathcal{H}}{\partial y_{\tau\tau}} \right) \right] \delta y \, d\tau \\
 & - \left[ \lambda \frac{\partial \mathcal{G}}{\partial x_\tau} \delta x - \frac{d}{d\tau} \left( \lambda \frac{\partial \mathcal{G}}{\partial x_{\tau\tau}} \right) \delta x \right]_0^1 - \left[ \lambda \frac{\partial \mathcal{G}}{\partial x_{\tau\tau}} \delta x_\tau \right]_0^1 \\
 & - \left[ \phi \frac{\partial \mathcal{H}}{\partial y_\tau} \delta y - \frac{d}{d\tau} \left( \phi \frac{\partial \mathcal{H}}{\partial y_{\tau\tau}} \right) \delta y \right]_0^1 - \left[ \phi \frac{\partial \mathcal{H}}{\partial y_{\tau\tau}} \delta y_\tau \right]_0^1.
 \end{aligned}$$

Now we use periodicity to simplify the boundary terms. Because  $x$  and  $y$  are node and saddle periodic orbits, and because  $F$  is assumed to be periodic with the same period, we have  $\delta x(0) \equiv \delta x(1)$ ,  $\delta x_\tau(0) \equiv \delta x_\tau(1)$ , etc. The same is true for  $y$ . The boundary terms simplify to

$$\begin{aligned}
 & - \left[ \frac{\partial \mathcal{G}}{\partial x_\tau} \delta x - \frac{d}{d\tau} \left( \frac{\partial \mathcal{G}}{\partial x_{\tau\tau}} \right) \delta x + \frac{\partial \mathcal{G}}{\partial x_{\tau\tau}} \delta x_\tau \right]_0 (\lambda(1) - \lambda(0)) \\
 & + \left[ \frac{\partial \mathcal{G}}{\partial x_{\tau\tau}} \delta x \right]_0 (\lambda'(1) - \lambda'(0)) \\
 & - \left[ \frac{\partial \mathcal{H}}{\partial y_\tau} \delta y - \frac{d}{d\tau} \left( \frac{\partial \mathcal{H}}{\partial y_{\tau\tau}} \right) \delta y + \frac{\partial \mathcal{H}}{\partial y_{\tau\tau}} \delta y_\tau \right]_0 (\phi(1) - \phi(0)) \\
 & + \left[ \frac{\partial \mathcal{H}}{\partial y_{\tau\tau}} \delta y \right]_0 (\phi'(1) - \phi'(0)).
 \end{aligned}$$

Thus, the boundary conditions disappear if we make the natural choice of  $\lambda$  and  $\phi$  periodic. It makes sense for  $\lambda$  and  $\phi$  to be periodic because they are Lagrange multipliers that enforce the constraints  $\mathcal{G} = 0$  and  $\mathcal{H} = 0$ , respectively. In the case of interest,  $x$ ,  $y$ , and the forcing that appear in the definitions of  $\mathcal{G}$  and  $\mathcal{H}$  are periodic. Hence, one can expect that because  $\mathcal{G}$  and  $\mathcal{H}$  are periodic, the associated Lagrange multipliers will be, also. Furthermore, it is convenient to let  $\lambda$  and  $\phi$  satisfy the equations obtained by setting to zero the coefficients of  $\delta x$  and  $\delta y$  in what is left,

$$\begin{aligned}
 \delta J = & \int_0^1 \left[ 2F - \lambda \frac{\partial \mathcal{G}}{\partial F} - \phi \frac{\partial \mathcal{H}}{\partial F} \right] \delta F - \mathcal{G} \delta \lambda - \mathcal{H} \delta \phi \\
 & + \left[ 2\mu(x-y) - \lambda \frac{\partial \mathcal{G}}{\partial x} + \frac{d}{d\tau} \left( \lambda \frac{\partial \mathcal{G}}{\partial x_\tau} \right) - \frac{d^2}{d\tau^2} \left( \lambda \frac{\partial \mathcal{G}}{\partial x_{\tau\tau}} \right) \right] \delta x \\
 & + \left[ -2\mu(x-y) - \phi \frac{\partial \mathcal{H}}{\partial y} + \frac{d}{d\tau} \left( \phi \frac{\partial \mathcal{H}}{\partial y_\tau} \right) - \frac{d^2}{d\tau^2} \left( \phi \frac{\partial \mathcal{H}}{\partial y_{\tau\tau}} \right) \right] \delta y \, d\tau.
 \end{aligned}$$

This leads to a set of Euler-Lagrange equations corresponding to the first variation of  $J$  being zero. First, we have the constraint equations, (10) and (11), which are the

coefficients of  $\delta\lambda$  and  $\delta\phi$  in  $\delta J$ . In addition, we have differential equations for the Lagrange multipliers

$$\frac{\omega^2}{36\pi^2} \frac{d^2\lambda}{d\tau^2} - \epsilon \frac{\omega k}{6\pi} \frac{d\lambda}{d\tau} + (\alpha + 3\epsilon x^2(\tau))\lambda(\tau) = 2\mu(x(\tau) - y(\tau)), \quad (14)$$

and

$$\frac{\omega^2}{36\pi^2} \frac{d^2\phi}{d\tau^2} - \epsilon \frac{\omega k}{6\pi} \frac{d\phi}{d\tau} + (\alpha + 3\epsilon y^2(\tau))\phi(\tau) = 2\mu(y(\tau) - x(\tau)), \quad (15)$$

which are the coefficients of  $\delta x$  and  $\delta y$ . Finally, we have the optimal control

$$F(\tau) = -(\lambda(\tau) + \phi(\tau))/2, \quad (16)$$

which is the coefficient of  $\delta F$ .

The goal, then, is to find simultaneous solutions of the equations (10), (11), (14), and (15) where the optimal modulation  $F$  is given by (16), and all dependent variables are periodic with period 1 in the variable  $\tau$ . The values of the various parameters used in the following calculations are:  $\epsilon = 0.1$ ,  $\alpha = 1$ ,  $k = 0.5$ ,  $\Gamma = 5$ , and  $\omega = 4.1$ . The value of  $\omega$  was chosen so as to capture the subharmonic resonance.

Now we turn to the numerical solution of the equations we have formulated. A conventional approach would employ the shooting method to determine the eight initial conditions required to find the periodic solutions for  $x(\tau)$ ,  $y(\tau)$ ,  $\lambda(\tau)$ , and  $\phi(\tau)$  by integrating the initial value problem. Instead we pursue an approach we introduced in an earlier paper [29], where we determined optimal controls and the periodic attractors they engender *together* by regarding the optimal control problem in the context of bifurcation theory. We use a continuation algorithm to follow the solutions of the system as we slowly vary any parameter, for example  $\mu$ . This approach has the advantage of allowing us to compute the periodic orbits directly, without having to go through the transient. The software AUTO94 [9] is instrumental in affording the opportunity to pursue this approach.

The key to beginning a continuation calculation is to have a solution of the full system available as a starting point. Here we are faced with some difficulties. It may be valuable for some readers to understand how these problems were addressed; we recount the details for their benefit.

A good starting point would be at  $\mu = 0$ , for then the Lagrange multipliers subsystem (14, 15) decouples from the two copies of the Duffing equation for the node periodic orbit  $x$  (10) and the saddle periodic orbit  $y$  (11). Now, the node periodic orbit  $x$  and the saddle periodic orbit  $y$  are born in a saddle-node bifurcation as one varies, for example,  $\omega$ . We cannot start the calculation at the trivial solution when  $\Gamma = 0$  because the two orbits we need ( $x$  and  $y$ ) do not bifurcate from the trivial branch—instead, they inhabit an *isola*. Therefore, we must obtain  $x$  and  $y$  by a labor-intensive integration of the initial value problem, until the decay of transients, starting from initial conditions that lead to the subharmonic. Of course, the saddle orbit  $y$  is unstable (both in forward and in reverse time!); it cannot be found by such means. Therefore we find the orbit  $x$ , and continue in the parameter  $\omega$  around the saddle-node bifurcation that connects them until we can compute the orbit  $y$  at the same value of  $\omega$ . The strategy now is to try and reduce to zero the difference between the two periodic orbits (12), allowing  $\mu$  to vary freely. Of

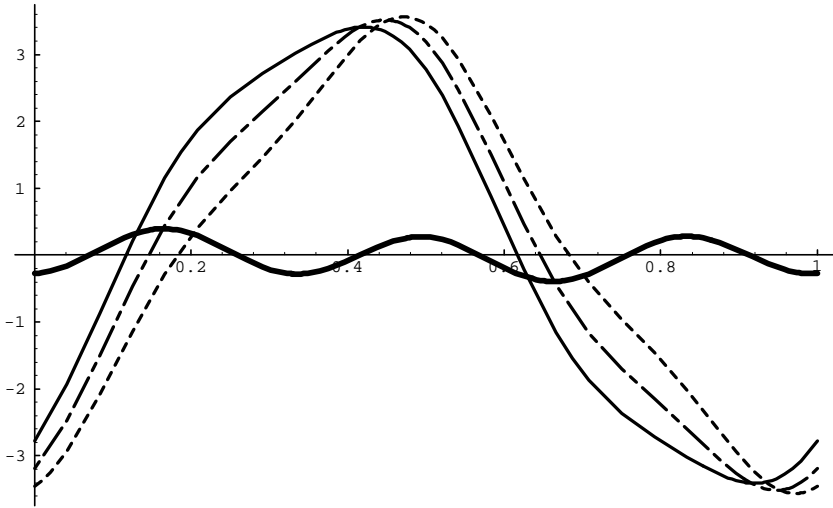


**Fig. 3.** Periodic solutions of the uncontrolled and controlled Duffing equation. The thin curves are the node (solid) and saddle (dashed) periodic orbits of the uncontrolled system (10, 11). When the optimal control is switched on, the node and saddle periodic orbits coalesce to form the nonhyperbolic orbit indicated by the dot-dashed curve. Finally, the thick solid curve is the attractor that takes over in the controlled system. The orbits are computed with  $\omega = 4.1$ , damping  $k = 0.5$ , and subharmonic forcing amplitude  $\Gamma = 5$ .

course, it is numerically impossible to reduce the difference to an exact zero. Several test calculations indicated that a value of  $10^{-6}$  for the  $L_2$ -norm (squared) of the difference (as defined in (12)) is sufficient.

In Figure 3 we show the relevant periodic responses. The thin curves are the node (solid) and saddle (dashed) periodic orbits of the uncontrolled system. When the optimal control is switched on, the node and saddle periodic orbits coalesce to form the nonhyperbolic orbit indicated by the dot-dashed curve in Figure 3. Finally, the thick solid curve is the attractor that takes over in the controlled system. Hence, the optimal control changes the response from the thin solid curve to the thick solid curve in Figure 3. The goal of reducing the response at the subharmonic resonance has been achieved by causing the system to undergo a saddle-node bifurcation of periodic orbits to eliminate the resonance.

These responses are driven by the subharmonic drive shown in Figure 4, and, in the case of the controlled system, by the modulation shown in Figure 5. The optimal control is essentially a small amplitude, phase-shifted component at one-third the frequency of the subharmonic drive, i.e., at the main harmonic.

The reader should be concerned that whatever replaces the annihilated subharmonic might be worse, as one might suspect that the system is much more susceptible to large amplitude responses when driven at the strong resonance. However, such is not the case. In Figure 6 we show the time evolution of the  $L_2$ -norm of the solution  $x(\tau)$  after switching on the optimal modulation at time  $\tau = 0$ . The solution is attracted by a much smaller amplitude periodic orbit.

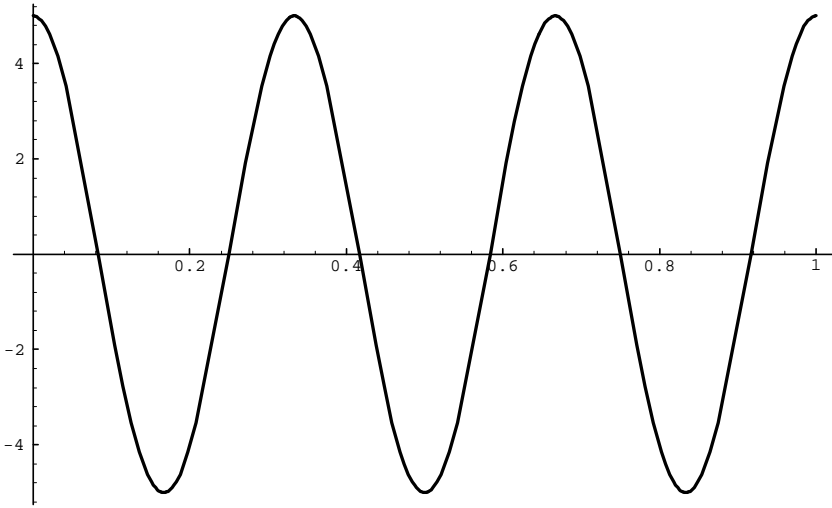


**Fig. 4.** This is the subharmonic drive that leads to the principal subharmonic—the thin, solid curve in Fig. 3, and its sister saddle periodic orbit—the thin dashed curve in Fig. 3.

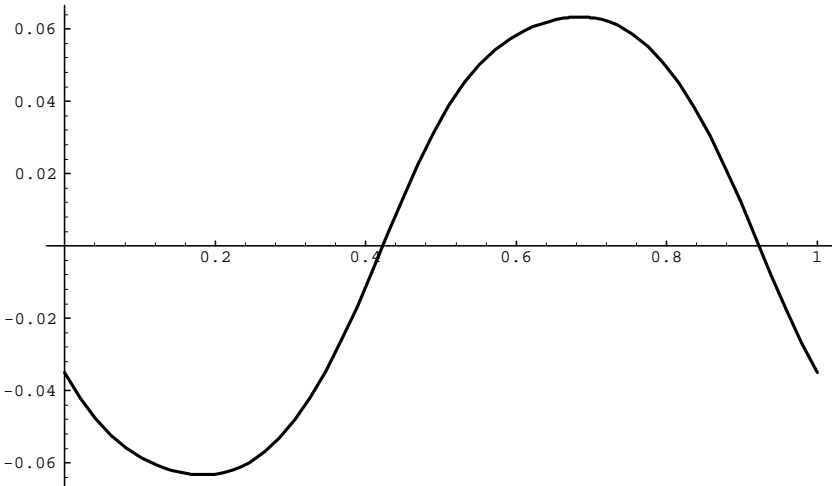


**Fig. 5.** When combined with the subharmonic drive shown in Fig. 4, this optimal modulation achieves the saddle-node bifurcation of periodic orbits  $x$  and  $y$  that annihilates the subharmonic response. This is the control that changes the attractor from the thin solid curve to the thick solid curve in Fig. 3. Projected onto a Fourier basis, the modulation is  $F(\tau) \approx -0.0317484 \cos 2\pi \tau - 0.0587489 \sin 2\pi \tau - 0.00382666 \cos 6\pi \tau + 0.00031538 \sin 6\pi \tau$ .

An energy method provides the most direct answer to the question of why a carefully chosen modulation has such power to affect the attractors in this system. We begin by multiplying (10) by  $dx/d\tau$  and setting the result equal to zero. After some manipulation,

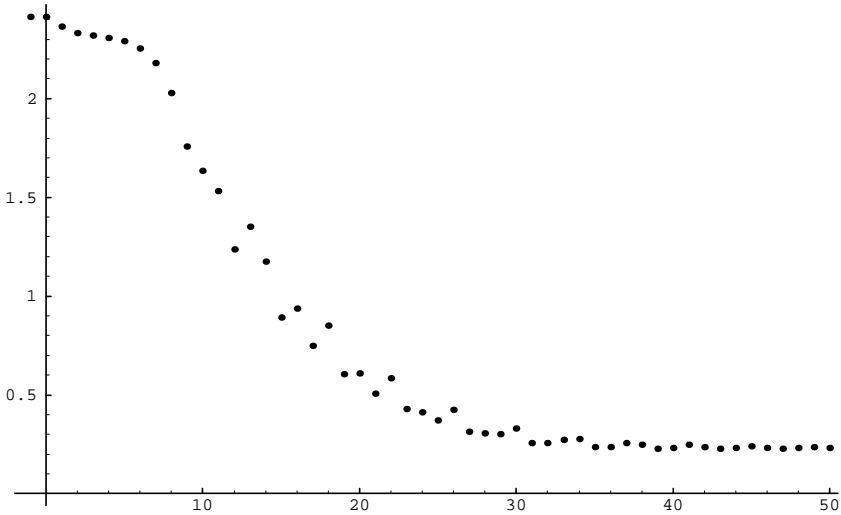


**Fig. 6.** A plot of the transient of the  $L_2$ -norm when the subharmonic resonance is destroyed by switching on the optimal control shown in Fig. 5 at  $\tau = 0$ . The new limit cycle in the controlled system is shown in Fig. 3 as a thick solid curve.

we obtain

$$\frac{d}{d\tau} \left[ \frac{\omega^2}{72\pi^2} \left( \frac{dx}{d\tau} \right)^2 + \frac{\alpha}{2} x^2 + \frac{\epsilon}{4} x^4 \right] = -\frac{\epsilon\omega k}{6\pi} \left( \frac{dx}{d\tau} \right)^2 + \Gamma \frac{dx}{d\tau} \cos(6\pi\tau) + F(\tau) \frac{dx}{d\tau}. \tag{17}$$

The term in square brackets can be interpreted as an energy; it is in fact the Hamiltonian of the unforced, undamped system. In an unforced system, the total energy decays with time by virtue of the damping term. Energy can be increased or decreased by forcing, proportional to  $\Gamma$ , and also by modulation  $F$ . If we consider for a moment a periodic attractor  $\bar{x}$ , then (17) provides a necessary condition for its existence,

$$\frac{\epsilon\omega k}{6\pi} \int_0^1 \left( \frac{d\bar{x}}{d\tau} \right)^2 d\tau = \Gamma \int_0^1 \frac{d\bar{x}}{d\tau} \cos(6\pi\tau) d\tau + \int_0^1 F(\tau) \frac{d\bar{x}}{d\tau} d\tau.$$

Hence, over a period, the net energy input by forcing and modulation is balanced by energy loss due to the dissipation. If one recalls from the weakly nonlinear analysis that the bulk of the response to driving at three times the natural frequency of the linearized oscillator is, nevertheless, at the natural frequency, it is clear why the modulation is able to extract energy from the system. This is because the modulation, multiplied by  $d\bar{x}/d\tau$ , extracts that component of the response at the main harmonic. This analysis would appear to indicate that noise would have little effect on such a system, as one can expect there would be little residue of the integral of  $F$  times  $d\bar{x}/d\tau$  when  $F$  is rapidly fluctuating with zero mean. Such arguments are further useful as a basis for a feedback control scheme. These ideas are the topic of ongoing inquiry.

#### 4.2. Control of the 2/1 Rayleigh-Plesset Ultraharmonic

Now we attempt the same feat with a principal ultraharmonic resonance. Because the ultraharmonic response of the Duffing equation is not substantial, a more interesting example is the Rayleigh-Plesset equation that governs the spherical oscillations of a single microbubble of radius  $R(\tilde{t})$ ,

$$R\ddot{R} + \frac{3}{2}\dot{R}^2 = \frac{1}{\rho} \left( p_{Gi} \left( \frac{a}{R} \right)^{3\eta} - (p_\infty - p_s(\omega\tilde{t}) - \tilde{F}(\tilde{t})) - \frac{2\gamma}{R} - \frac{4\mu\dot{R}}{R} \right). \quad (18)$$

Here,  $\rho$  is the density of the liquid,  $p_s$  is the pressure due to the driving sound field,  $p_\infty$  is atmospheric pressure,  $\tilde{F}(\tilde{t})$  is the pressure due to the controlling sound field (the modulation),  $\gamma$  is the interfacial tension, and  $\mu$  is the viscosity of the liquid. The polytropic exponent  $\eta$  varies between the extremes of unity for an isothermal bubble and the ratio of specific heats  $c_p/c_v$  for an adiabatic bubble. We use a tilde where necessary to distinguish a dimensional variable. For a derivation and general introduction to the dynamics of the Rayleigh-Plesset equation, the interested reader may consult Leal [17]. This equation exhibits large sharp ultraharmonics (Lauterborn [16]). This simple model is not the best one for resonantly forced bubble dynamics [10], but it is fine for illustrative purposes.

The problem may be nondimensionalized with respect to the following natural scales. As a length scale, we take  $a$ , the radius of the undisturbed bubble. The time scale is  $\Omega_0^{-1}$ , which is the inverse of the natural frequency of radial oscillations of the bubble about the undisturbed state. Pressure is made dimensionless using the pressure scale  $\frac{1}{2}\rho a^2 \Omega_0^2$ . This leads to dimensionless parameters corresponding to the Weber number  $\mathcal{W}$ ,

$$\mathcal{W} = \frac{2\rho(a\Omega_0)^2 a}{\gamma},$$

the Reynolds number  $\mathcal{R}$ ,

$$\mathcal{R} = \frac{\rho(a\Omega_0)a}{\mu},$$

and a parameter related to the internal pressure of the undisturbed bubble  $p_{Gi}^*$ . See Fyrrillas and Szeri [10] for more details on the nondimensionalization. In what follows we shall control the ultraharmonic resonance of an  $a = 10 \mu\text{m}$  air bubble in water, at atmospheric pressure  $p_\infty = 10^6 \text{ dyne/cm}^2$ . The surface tension is  $\gamma = 72.8 \text{ dyne/cm}$ . For the polytropic exponent, we take  $\eta = 1.33$ .

As in the control scheme for the Duffing subharmonic, we shall require two copies of the Rayleigh-Plesset equation: one for the node periodic orbit and another for the sister saddle periodic orbit. In this case, however, it is convenient to transform these equations into a first-order system. Also, we recast the problem onto a unit time interval by defining  $\omega\tilde{t} = (\omega/\Omega_0)t \equiv 2\pi\tau$ . In terms of these definitions, the equations satisfied by the node periodic orbit  $x_1(\tau)$  and  $x_2(\tau)$  may be written  $\mathcal{G}_1 = 0$  and  $\mathcal{G}_2 = 0$ , where:

$$\mathcal{G}_1(x_1, x_2) \equiv \frac{dx_1}{d\tau} - \frac{2\pi x_2}{\omega/\Omega_0}, \quad (19)$$

$$\mathcal{G}_2(x_1, x_2) \equiv \frac{dx_2}{d\tau} - \frac{2\pi}{\omega/\Omega_0} \frac{1}{2x_1} \times \left[ -3x_2^2 + p_{Gi}^* x_1^{-3\eta} - \frac{8}{x_1 \mathcal{W}} - \frac{8x_2}{x_1 \mathcal{R}} - p_\infty^* (1 - \Gamma \cos(2\pi\tau) - F(\tau)) \right]. \quad (20)$$

There is another set of identical equations satisfied by  $y_1(\tau)$  and  $y_2(\tau)$ , for the saddle periodic orbit; we call these  $\mathcal{H}_1 = 0$  and  $\mathcal{H}_2 = 0$ . The unforced system has the solution  $x_1 = 1$ ,  $x_2 = 0$ ,  $y_1 = 1$ , and  $y_2 = 0$ .

The goal of the optimization problem is the same as for our control of the Duffing subharmonic; we want to reduce to zero the difference between the node and saddle periodic orbits,

$$\int_0^1 (x_1(\tau) - y_1(\tau))^2 d\tau, \quad (21)$$

using a minimum modulation, as measured by

$$\int_0^1 F^2(\tau) d\tau.$$

To accomplish this task, we form the function

$$J = \int_0^1 [\mu (x_1 - y_1)^2 + F^2 - \lambda_1 \mathcal{G}_1 - \lambda_2 \mathcal{G}_2 - \phi_1 \mathcal{H}_1 - \phi_2 \mathcal{H}_2] d\tau.$$

Again,  $\mu$  plays the same role as in (13); the variables  $\lambda_i$  and  $\phi_i$  are the time-dependent Lagrange multipliers to enforce the differential constraints imposed by the governing equations.

Unlike the Duffing subharmonic treated in Section 4.1, attempting to find  $F(\tau)$  as an arbitrary periodic function is not so productive. It seems that strongly nonlinear oscillations governed by the Rayleigh-Plesset equation feature deep, sharp cusps which require many, many Fourier modes to resolve. Each of these modes excites a mode in the control  $F(\tau)$  which becomes hopelessly complicated. This is an area of ongoing investigation, but for the present we offer a simple alternative stratagem that is more practical. We limit  $F(\tau)$ , to the (detuned) harmonic Fourier component and optimize for the amplitudes; i.e., we set

$$F(\tau) = \alpha_2 \cos(4\pi\tau) + \beta_2 \sin(4\pi\tau),$$

which leads to

$$\int_0^1 F^2(\tau) d\tau = (\alpha_2^2 + \beta_2^2)/2. \quad (22)$$

A suitable cost function is

$$J = \int_0^1 [\mu (x_1 - y_1)^2 + \alpha_2^2 + \beta_2^2 - \lambda_1 \mathcal{G}_1 - \lambda_2 \mathcal{G}_2 - \phi_1 \mathcal{H}_1 - \phi_2 \mathcal{H}_2] d\tau.$$

In the case of the Duffing subharmonic, we searched over all possible modulations  $F(\tau)$  for that which was most effective at causing the saddle-node bifurcation of periodic orbits.

We found the most effective  $F(\tau)$  was a modulation at (roughly) the main harmonic. Now to control the Rayleigh-Plesset ultraharmonic, we are restricting  $F(\tau)$  to be (roughly) the main harmonic and simply optimizing over the phase. Actually, this is a slight oversimplification of the present approach, as will soon become evident.

A necessary condition for  $J$  to have a minimum is that its first variation should be zero. We regard everything else as fixed and imagine varying  $\alpha_2$  and  $\beta_2$ . Of course, when  $\alpha_2$  and  $\beta_2$  change, so also do the node and saddle periodic orbits ( $x_1, x_2, y_1$ , and  $y_2$ ) and also the time-dependent Lagrange multipliers ( $\lambda_1, \lambda_2, \phi_1$ , and  $\phi_2$ ). As before, we assume that each of these is periodic.

Following the development in Section 4.1, the coefficients multiplying variations of  $x_1, x_2, y_1$ , and  $y_2$  lead to differential equations for the Lagrange multipliers  $\lambda_1, \lambda_2, \phi_1$ , and  $\phi_2$ , respectively. Unlike the previous development, variations with respect to  $\alpha_2$  and  $\beta_2$  lead to *integral* constraints that should be satisfied at the minimum.

Thus, the Euler-Lagrange equations corresponding to  $\delta J = 0$  include the system of four differential equations for the node and saddle periodic orbits, and the differential equations for the Lagrange multipliers  $\lambda_1, \lambda_2, \phi_1$ , and  $\phi_2$ ,

$$\begin{aligned} \frac{\omega/\Omega_0}{2\pi} \frac{d\lambda_1}{d\tau} &= 2\mu(x_1 - y_1) \\ &\quad - \frac{\lambda_2}{2x_1} \left[ -3\eta p_{Gi}^* x_1^{-1-3\eta} + \frac{8x_2}{x_1^2 \mathcal{R}} + \frac{8}{x_1^2 \mathcal{W}} \right] \\ &\quad + \frac{\lambda_2}{2x_1^2} \left[ \frac{p_{Gi}^*}{x_1^{3\eta}} - \frac{8x_2}{x_1 \mathcal{R}} - 3x_2^2 - \frac{8}{x_1 \mathcal{W}} - p_\infty^* (1 - \Gamma \cos(4\pi \tau) - F(\tau)) \right], \end{aligned} \quad (23)$$

$$\frac{\omega/\Omega_0}{2\pi} \frac{d\lambda_2}{d\tau} = -\lambda_1 + \frac{\lambda_2}{2x_1} \left( \frac{8}{x_1 \mathcal{R}} + 6x_2 \right), \quad (24)$$

$$\begin{aligned} \frac{\omega/\Omega_0}{2\pi} \frac{d\phi_1}{d\tau} &= -2\mu(x_1 - y_1) \\ &\quad - \frac{\phi_2}{2y_1} \left[ -3\eta p_{Gi}^* y_1^{-1-3\eta} + \frac{8y_2}{y_1^2 \mathcal{R}} + \frac{8}{y_1^2 \mathcal{W}} \right] \\ &\quad + \frac{\phi_2}{2y_1^2} \left[ \frac{p_{Gi}^*}{y_1^{3\eta}} - \frac{8y_2}{y_1 \mathcal{R}} - 3y_2^2 - \frac{8}{y_1 \mathcal{W}} - p_\infty^* (1 - \Gamma \cos(4\pi \tau) - F(\tau)) \right], \end{aligned} \quad (25)$$

$$\frac{\omega/\Omega_0}{2\pi} \frac{d\phi_2}{d\tau} = -\phi_1 + \frac{\phi_2}{2y_1} \left( \frac{8}{y_1 \mathcal{R}} + 6y_2 \right), \quad (26)$$

respectively. The integral constraints arising from variations of  $\alpha_2$  and  $\beta_2$  are

$$\int_0^1 \left[ 2\alpha_2 - \frac{p_\infty^* \lambda_2 \cos(4\pi \tau)}{2x_1} - \frac{p_\infty^* \phi_2 \cos(4\pi \tau)}{2y_1} \right] d\tau = 0, \quad (27)$$

$$\int_0^1 \left[ 2\beta_2 - \frac{p_\infty^* \lambda_2 \sin(4\pi \tau)}{2x_1} - \frac{p_\infty^* \phi_2 \sin(4\pi \tau)}{2y_1} \right] d\tau = 0, \quad (28)$$

respectively.

Now we turn to the numerical solution of this problem. We shall make use of the *successive continuation strategy* developed by Doedel et al. [8] for optimization of a scalar function of the solution of an ordinary differential equation over the choice of several parameters.

The key ideas are the following. When we have forced the saddle-node bifurcation of periodic orbits, the norm of  $x_1 - y_1$  is zero. Because  $x_i$  and  $y_i$  satisfy their respective differential equations,  $\mathcal{G}_i$  and  $\mathcal{H}_i$  are zero. Hence, the cost function becomes

$$J \rightarrow \alpha_2^2 + \beta_2^2.$$

The goal is to drive  $J$  to be as small as possible, based on the best choice of  $\alpha_2$  and  $\beta_2$ , while satisfying *all* the constraints. There are a great many constraints to be satisfied simultaneously. The idea behind the successive continuation strategy is to satisfy one constraint at a time, while holding the previously satisfied constraints true. In this problem, the calculation goes as follows.

First, we obtain the node periodic orbit and the saddle periodic orbit of the uncontrolled system. There is no need for integration of an initial value problem to obtain the node periodic orbit because, unlike the Duffing subharmonic we examined, the present ultraharmonic is connected to the trivial branch. Thus, the starting point is the decoupled system with  $\mu = 0$ ,  $\lambda_1$ ,  $\lambda_2$ ,  $\phi_1$ , and  $\phi_2$  all zero. The integral constraints (27, 28) are trivially satisfied.

Next, we vary the value of  $\|x_1 - y_1\|_2^2$ , allowing  $\mu$ ,  $\alpha_2$ , and the value of the integral (28) to float freely. We maintain  $\beta_2 = 0$ . The continuation procedure is started, by choosing a negative step size for  $\|x_1 - y_1\|_2^2$ —thus forcing  $\|x_1 - y_1\|_2^2$  to decrease. When we decrease  $\|x_1 - y_1\|_2^2$ , the parameter  $\mu \neq 0$ , meaning that the systems for the Lagrange multipliers become coupled. The integral constraint (27) is enforced throughout; hence, the cost function

$$J = \int_0^1 [\mu(x_1 - y_1)^2 + \alpha_2^2] d\tau$$

always has a minimum with respect to variations in  $\alpha_2$  as we decrease  $\|x_1 - y_1\|_2^2$ . At the point where  $\|x_1 - y_1\|_2^2$  is zero,<sup>1</sup> we thus obtain the minimum value of  $\alpha_2$  that achieves the saddle-node bifurcation.

The saddle-node bifurcation has been achieved with the smallest possible modulation of the ultraharmonic drive by mixing in the main harmonic via  $\alpha_2 \neq 0$ . However, we have not optimized with respect to the phase of the modulation at the main harmonic. To do this, we would like to further decrease

$$J = \int_0^1 [\alpha_2^2 + \beta_2^2] d\tau,$$

by allowing  $\beta_2 \neq 0$ . The procedure is as follows. Now we decrease  $\|F(\tau)\|_2^2$  directly, allowing  $\alpha_2$ ,  $\beta_2$ , and  $\mu$  to vary freely. The integral constraint (27) is enforced throughout—so we do not have to give up the hard-won gain of having optimized  $J$  over the choice

<sup>1</sup> Actually,  $\|x_1 - y_1\|_2^2 = 10^{-6}$  to be precise.

**Table 1.** Values of the cost function at steps along the successive continuation strategy to force a saddle-node bifurcation to eliminate the Rayleigh-Plesset principal ultraharmonic with minimum modulation of the drive.

Step	I	II	III	IV
$J$	$1.087980 \times 10^{-5}$	$1.087842 \times 10^{-5}$	$1.045380 \times 10^{-5}$	$9.877780 \times 10^{-6}$
$\alpha_2$	$-3.298454 \times 10^{-3}$	$-3.298046 \times 10^{-3}$	$-3.170122 \times 10^{-3}$	$-2.994910 \times 10^{-3}$
$\beta_2$	0	$3.619523 \times 10^{-5}$	$1.934026 \times 10^{-5}$	$2.559549 \times 10^{-5}$
$\alpha_3$	0	0	$6.354150 \times 10^{-4}$	$6.040325 \times 10^{-4}$
$\beta_3$	0	0	0	$7.367375 \times 10^{-4}$

of  $\alpha_2$ . We also enforce  $\|x_1 - y_1\|_2^2 = 0$  throughout. This may be regarded as another integral constraint that we satisfied previously. As we decrease  $\|F(\tau)\|_2^2$  directly, the value of the integral on the left-hand side of (28) will vary continuously. When this integral takes the value zero, and hence when the corresponding integral constraint is satisfied, we have found a local extremum of the cost function with respect to  $\alpha_2$  and  $\beta_2$ . Because we have never given up  $\|x_1 - y_1\|_2^2 = 0$ , this most-efficient combination  $\alpha_2$  and  $\beta_2$  forces a saddle-node bifurcation of the Rayleigh-Plesset principal ultraharmonic. Thus, we have modulated the ultraharmonic drive by a component at the main harmonic, suitably optimized with respect to both amplitude and phase. These arguments constitute a simpler finite-dimensional version of the optimal control problem we developed and solved for the Duffing subharmonic.

In Table 1 we list the values of the cost function  $J$  at various steps along the way in the successive continuation strategy. Actually, we performed this optimal control problem including another complete Fourier component of modulation,

$$F(\tau) = \alpha_2 \cos(4\pi\tau) + \beta_2 \sin(4\pi\tau) + \alpha_3 \cos(6\pi\tau) + \beta_3 \sin(6\pi\tau), \quad (29)$$

just to demonstrate that this is possible. The arguments for this successive continuation strategy are a straightforward extension of the previous development. One observes in Table 1 that each time we allow the ultraharmonic drive to be modulated by a yet more complicated control  $F(\tau)$ , the cost function  $J = \|F(\tau)\|_2^2$  takes a smaller value. Note that these values of the control are two orders of magnitude smaller than the ultraharmonic drive.

In Figure 7 we show the relevant periodic responses. The thin curves are the node (solid) and saddle (dashed) periodic orbits of the uncontrolled system. When the optimal control is switched on, the node and saddle periodic orbits coalesce to form the non-hyperbolic orbit indicated by the dot-dashed curve in Figure 7. Finally, the thick solid curve is the attractor that takes over in the controlled system. Recall that the *unforced* bubble radius is  $x_1 = 1$ ; therefore the limit cycle of the controlled system has a very small amplitude indeed. Hence, as in the Duffing subharmonic, the optimal control changes the response from the thin solid curve to the thick solid curve in Figure 7. The goal of reducing the response at the principal ultraharmonic resonance has been achieved by causing the system to undergo a saddle-node bifurcation of periodic orbits to eliminate the resonance. This was accomplished by an optimal modulation of the ultraharmonic drive.

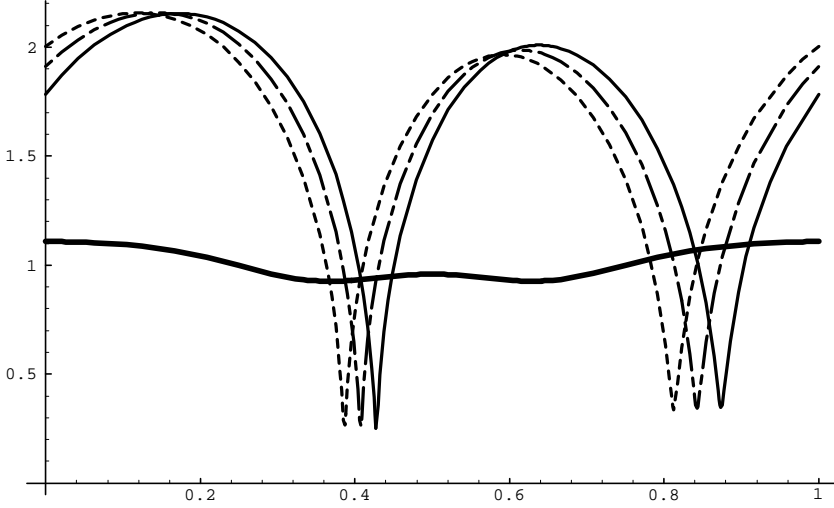


**Fig. 7.** Periodic solutions of the uncontrolled and controlled Rayleigh-Plesset equation. The thin curves are the node (solid) and saddle (dashed) periodic orbits of the uncontrolled system. When the optimal control is switched on, the node and saddle periodic orbits coalesce to form the nonhyperbolic orbit indicated by the dot-dashed curve. Finally, the thick solid curve is the attractor that takes over in the controlled system. Note that the bubble radius is  $x_1(\tau) = 1$  in the unforced system. The orbits are computed with  $\omega/\Omega_0 = 0.38$  and ultraharmonic forcing amplitude  $\Gamma = 0.33$ . These results are for the principal ultraharmonic resonance of an acoustically forced  $10 \mu\text{m}$  air bubble in water.

These responses are forced by the ultraharmonic drive shown in Figure 8, and, in the case of the controlled system, by the modulation shown in Figure 9. In Figure 10, we show the time evolution of the  $L_2$ -norm of the solution  $x(\tau)$  after switching on the optimal forcing at time  $\tau = 0$ . The solution is attracted by the smaller amplitude periodic orbit shown in Figure 7 as a thick solid line. Note that the new attractor has no cusps!

As in the case of the Duffing subharmonic, the efficacy of the modulation in reducing the response can be understood readily from an energy argument. We multiply (18) by  $R^2 \dot{R}$  and rearrange to obtain

$$\frac{d}{d\tilde{t}} \left[ \frac{R^3 \dot{R}^2}{2} + \frac{p_{Gi} a^{3\eta}}{(3\eta - 3)\rho R^{3\eta-3}} + \frac{p_\infty R^3}{3\rho} + \frac{\gamma R^2}{\rho} \right] = -\frac{4\mu}{\rho} R \dot{R}^2 + \frac{p_s + \tilde{F}}{\rho} R^2 \dot{R}. \quad (30)$$

When  $\eta = 1$  (isothermal bubble), we remark that the term multiplied by  $p_{Gi}$  involves instead the logarithm of  $1/R$ . The term in square brackets is the Hamiltonian for the case of undamped, unforced dynamics.<sup>2</sup> As for the Duffing equation, restriction of (30) to the case of a periodic attractor yields a necessary condition for its existence involving the balance of net energy transfer to the bubble over a cycle of oscillation with the energy

<sup>2</sup> The canonical variables are  $R$  and  $R^3 \dot{R}$ .

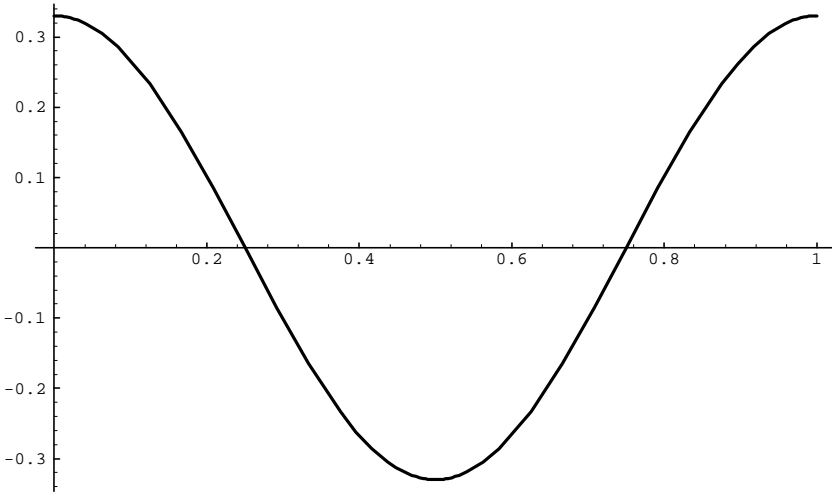


**Fig. 8.** A plot of the forcing that drives the principal ultraharmonic—the thin, solid curve in Fig. 7, and its sister saddle periodic orbit—the thin dashed curve in Fig. 7.

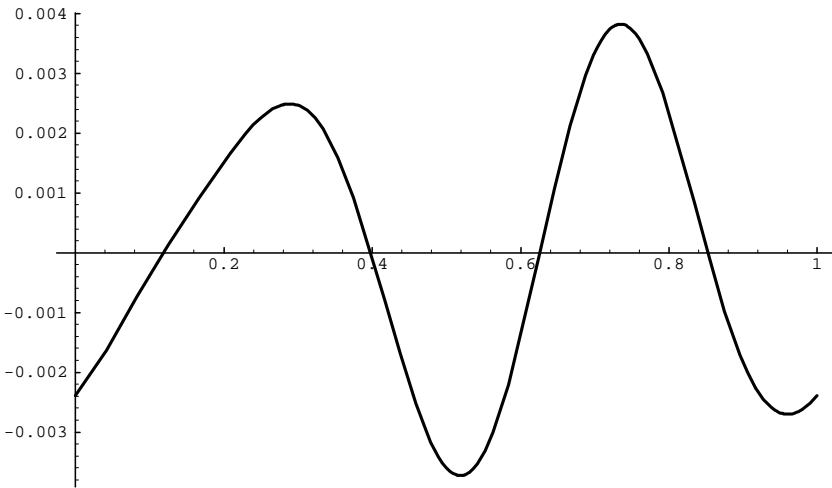


**Fig. 9.** When combined with the subharmonic drive shown in Fig. 8, this optimal modulation  $F(\tau) = -0.00299491 \cos 4\pi\tau + 0.0000255955 \sin 4\pi\tau + 0.0006040325 \cos 6\pi\tau + 0.0007367375 \sin 6\pi\tau$  achieves the saddle-node bifurcation of periodic orbits  $x$  and  $y$  that annihilates the ultraharmonic response. This is the control that changes the attractor from the thin solid curve to the thick solid curve in Fig. 7.

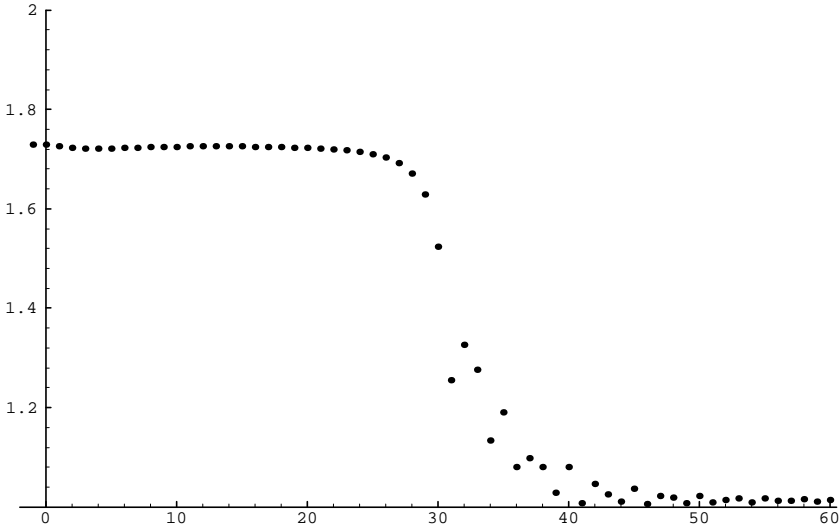


**Fig. 10.** A plot of the transient of the  $L_2$ -norm when the ultraharmonic resonance of the Rayleigh-Plesset equation is destroyed by switching on the optimal control shown in Fig. 9 at  $\tau = 0$ . The new limit cycle is shown in Fig. 7 as a thick solid curve.

loss by viscous damping,

$$\frac{4\mu}{\rho} \int_0^{\tilde{T}} \bar{R} \dot{\bar{R}}^2 d\tilde{t} = \frac{1}{\rho} \int_0^{\tilde{T}} p_s \bar{R}^2 \dot{\bar{R}} d\tilde{t} + \frac{1}{\rho} \int_0^{\tilde{T}} \tilde{F} \bar{R}^2 \dot{\bar{R}} d\tilde{t}. \quad (31)$$

From a thermodynamic point of view, the net energy transfer to the bubble has the nice interpretation of the integral of  $p dv$  work. Finally, it is clear that modulation at the main harmonic is effective at controlling an attractor supported by forcing at half the frequency because the primary component of the uncontrolled response is at the main harmonic; this energy of this part is readily extracted by the modulation.

## 5. Direct Manipulation of Response Diagrams

Thus far, we have considered problems at a fixed value of the detuning. We began with weak nonlinearity (and hence weak detuning) that admitted a multiple-scales analysis. In this setting, we could think of the control as forcing the saddle-node bifurcation of fixed points in the system for the slowly varying amplitudes. Next, we considered strong nonlinearity (and hence large detuning). This forced us to confront the fact that the bifurcations we were causing were in fact saddle-node bifurcations of periodic orbits in the full three-dimensional phase space (the product  $(x, x_\tau)$ -plane and the circle for the phase of the forcing). Now we shall allow our point of view to evolve further to consider the response diagram itself.

As we have mentioned, the ultra- and subharmonic resonances are born (or die) at saddle-node bifurcations of periodic orbits as one varies the detuning. One interesting take on what has been accomplished thus far is that the modulation has the effect of

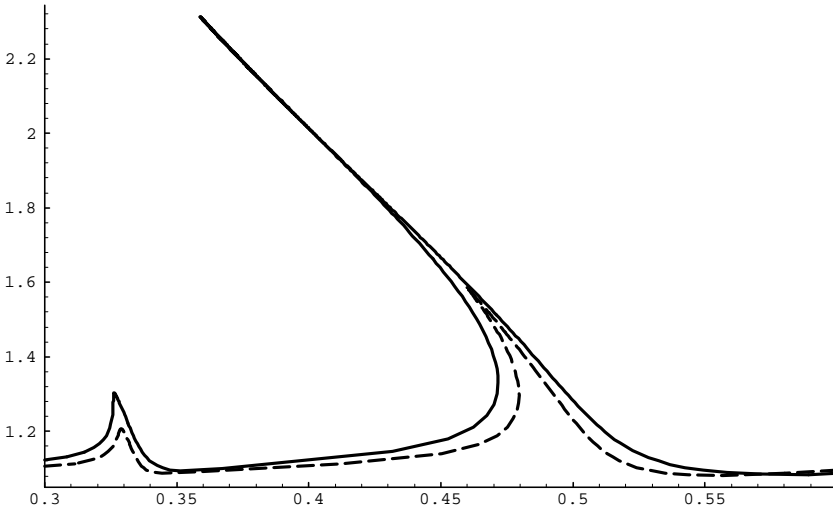


**Fig. 11.** Response diagram of the uncontrolled (solid curve) and the controlled (dashed curve) principal ultraharmonic of the Rayleigh-Plesset equation. The plot shows the maximum of the dimensionless bubble radius on the limit cycle versus the ratio between the driving frequency and the natural frequency. The limit point at the upper extreme of the resonance peak was moved from  $\omega/\Omega_0 \approx 0.36$  in the uncontrolled system to  $\omega/\Omega_0 = 0.46$  in the controlled system, using the technique of choosing optimal modulation by a few Fourier modes. The solid curve represents the response diagram of (19, 20) with forcing amplitude  $\Gamma = 0.33$ , while the dashed curve is the response diagram for the same system with the forcing  $\Gamma = 0.33$  modulated by  $F(\tau) = -0.02817305 \cos 4\pi\tau + 0.0001998301 \sin 4\pi\tau + 0.006122100 \cos 6\pi\tau + 0.005069228 \sin 6\pi\tau$ . These results are for the principal ultraharmonic resonance of an acoustically forced  $10 \mu\text{m}$  air bubble in water.

shifting the location of important saddle-node bifurcations with respect to the detuning. Rather than considering this as just another point of view, we shall now take this as a plan. We shall attempt to move the saddle-node bifurcations that limit the ultra- and subharmonic resonances.

Once again we make use of (29) to force a saddle-node bifurcation to eliminate the principal ultraharmonic response of the Rayleigh-Plesset equation. This time, we force the saddle-node bifurcation to occur at  $\omega/\Omega_0 = 0.46$ , and obtain the parameters  $\alpha_2 = -0.02817305$ ,  $\beta_2 = 0.0001998301$ ,  $\alpha_3 = 0.006122100$ , and  $\beta_3 = 0.005069228$ . It is no surprise that to force the saddle-node bifurcation at this driving frequency “costs more” compared to  $\omega/\Omega_0 = 0.38$  (see Table 1) because the saddle and node periodic orbits of the unperturbed system are further apart.

Now, we use this modulation not just at  $\omega/\Omega_0 = 0.46$  to annihilate the ultraharmonic, but over a range of  $\omega/\Omega_0$  to compute the response diagram. This is shown in Figure 11. One observes that the saddle-node bifurcation that limits the maximum ultraharmonic response in the uncontrolled system (solid curve) is moved quite effectively in the controlled system. Hence, the controlling modulations we develop are useful in softening catastrophic bifurcations and in reducing or eliminating hysteresis.

We remark that it is also straightforward to enhance the resonance by moving the

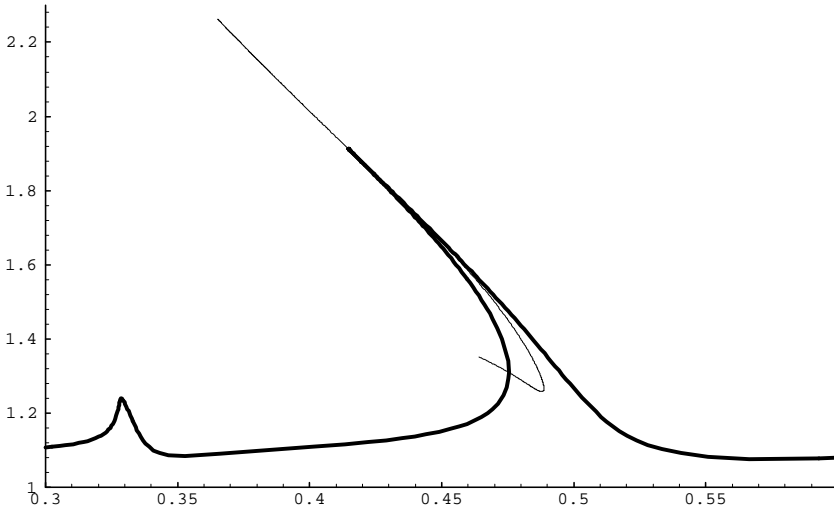


**Fig. 12.** Response diagram of the Rayleigh-Plesset equation (20) with  $\Gamma = 0.3$ . The fine curve indicates the locus of the limit points as the amplitude of the harmonic modulation ( $F_0 \cos 4\pi\tau$ ) is changed from zero. For positive values of  $F_0$ , the limit points shift to the left, while for negative  $F_0$  both limit points shift to the right. For large-enough negative  $F_0$ , the limit point coalesce as shown in Fig. 13.

saddle-node bifurcation that limits the response to the left, as discussed in the following paragraph. In addition, it is possible to reduce or to eliminate the isola in the response diagram of the principal subharmonic of the Duffing equation.

The fact that we were able to shift the saddle-node bifurcations with respect to the detuning leads to an alternative technique for developing a suitable control. This essentially involves the enforcement of (31) while subtracting energy from the attractor by increasing the modulation. The control can be found from a two-parameter continuation of limit points, one parameter being the detuning and the other the amplitude of the modulation; we limit the present discussion only to the harmonic component of the modulation  $F_0 \cos 4\pi\tau$ . In Figure 12, the heavy curve is the response of the Rayleigh-Plesset equation to a forcing of amplitude  $\Gamma = 0.3$ , i.e.,  $0.3 \cos 2\pi\tau$ . The fine curve shows the locus of the limit points in the response diagram as one changes  $F_0$  from zero. For positive values of  $F_0$ , the limit points shift to the left, thus enhancing the peak resonance, whereas for negative values, both limit points shift to the right and finally coalesce, shown in detail as a cusp in Figure 13. For values of  $F_0 < -0.041$ , the  $2/1$  ultraharmonic has no limit points and is similar to the  $3/1$  ultraharmonic.

## 6. Conclusion

We have shown that it is possible, by subtle modulation of the forcing of a nonlinear oscillator, to destroy ultra- and subharmonic resonances. What survives is a smaller-amplitude periodic attractor. This may be understood in a weakly nonlinear setting using

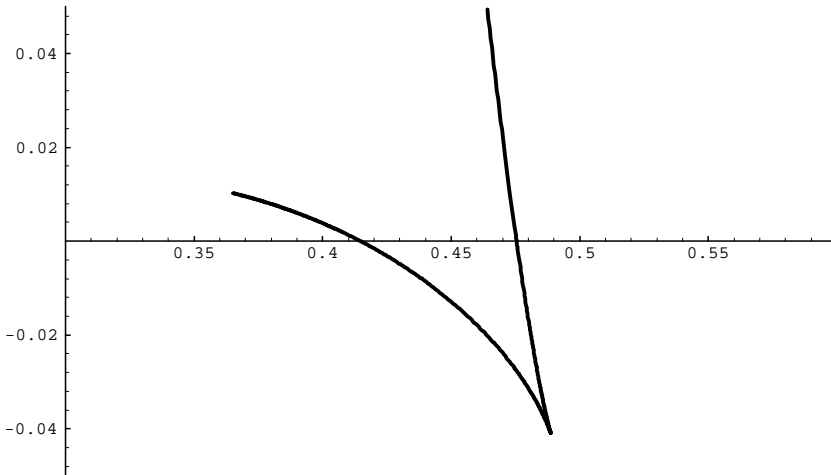


**Fig. 13.** An alternative view of the two-parameter continuation of the limit points (amplitude of harmonic modulation versus frequency) for the Rayleigh-Plesset equation (equivalent to the fine line in Fig. 12). The curve shows the locus of the limit points as a function of the frequency as the modulation amplitude is varied from zero. At the cusp, the two limit points coalesce.

the method of multiple scales, and approached numerically using optimal control theory in either an infinite or a finite dimensional setting. Remarkably, what is required to destroy the resonances emerges as modulation of the ultra- or subharmonic drive with a component at the main harmonic. Of course, forcing at the main harmonic is normally associated with the strongest resonant response of which the system is capable—but in the present context, this extra forcing reduces the response.

The methods we have developed are naturally grouped with other work at modifying bifurcations described in Section 2. However, our focus is on bifurcations of attractors of periodically forced systems; moreover, we try to exploit what we know of the geometry of the unperturbed systems in new ways. Our work on the optimal control problem to control the principal ultraharmonic resonance of the Rayleigh-Plesset equation makes use of some optimization techniques of Doedel et al. [8]. The optimal control of the Duffing principal subharmonic we present is considerably different, as we are optimizing in a function space, not in finite dimensional space. The variational techniques we used to derive optimal controls for the Duffing equation recall those of Wargitsch and Hübler [33]. However, the goals of our optimization problems are different: manipulation of the geometrical structure of the system instead of maximizing the response.

Viewed, perhaps, with a little more perspective, this work suggests a new point of view on the relationship between control theory and nonlinear dynamics. By understanding how a system can respond to continuous changes in parameters (including forcing), one opens up the possibility of using optimal control theory for direct manipulation of global structures in the geometry of the system.

## Acknowledgments

The authors would like to thank M. Brenner, A. Champneys, E. Doedel, Y. Kuznetsov, K. Mease, and W. E. Schmitendorf for helpful discussions and I. Kevrekidis for guidance on previous work in this area. This research was supported by a Young Investigator Award to A. J. S. from the Office of Naval Research.

## References

1. E. H. Abed & J.-H. Fu, Local feedback stabilization and bifurcation control, I. Hopf bifurcation, *Syst. Control Lett.* **7** (1986) 11–17.
2. A. A. Atchley & L. A. Crum, Acoustic cavitation and bubble dynamics, in *Ultrasound: Its Chemical, Physical and Biological Effects*, ed. by K. S. Suslick (VCH Publishers, New York, 1988).
3. P. Bryant & K. Wiesenfeld, Suppression of period-doubling and nonlinear parametric effects in periodically perturbed systems, *Phys. Rev. A* **33**(4) (1986) 2525–2543.
4. J. H. Chen, B. J. Cantwell, & N. N. Mansour, The effect of Mach number on the stability of a plane supersonic wake, *Phys. Fluids A* **2**(6) (1990) 984–1004.
5. C. C. Church, Prediction of rectified diffusion during nonlinear bubble pulsations at biomedical frequencies, *J. Acoust. Soc. Am.* **83** (1988) 2210–2217.
6. F. d'Auria, L. d'Agostino, & C. E. Brennen, Bubble dynamics effects on the rotordynamic forces in cavitating inducers, ASME Cavitation and Flow Forum (1995).
7. E. A. Doedel, H. B. Keller, & J. P. Kernevez, Numerical analysis and control of bifurcation problems (I) Bifurcation in finite dimensions, *Int. J. Bifurc. Chaos* **1**(3) (1991) 493–520.
8. E. A. Doedel, H. B. Keller, & J. P. Kernevez, Numerical analysis and control of bifurcation problems (II) Bifurcation in infinite dimensions, *Int. J. Bifurc. Chaos* **1**(4) (1991) 745–772.
9. E. A. Doedel, X. Wang, & T. Fairgrieve, *AUTO94: Software for continuation and bifurcation problems in ordinary differential equations*. California Institute of Technology Applied Mathematics Report (1994).
10. M. M. Fyrillas & A. J. Szeri, Dissolution or growth of soluble spherical oscillating bubbles, *J. Fluid Mech.* **277** (1994) 381–407.
11. C. Hayashi, *Nonlinear Oscillations in Physical Systems* (McGraw-Hill, New York, 1964).
12. C.-M. Ho & L. Huang, Subharmonics and vortex merging in mixing layers, *J. Fluid Mech.* **119** (1982) 443–473.
13. K. Kawashima & O. B. Wright, Resonant electromagnetic excitation and detection of ultrasonic waves in thin sheets, *J. Appl. Phys.* **72**(10) (1992) 4830–4839.
14. K. Kawashima, O. B. Wright, & T. Hyoguchi, High frequency resonant electromagnetic generation and detection of ultrasonic waves, *Jpn. J. Appl. Phys.* **33**(1) No. 5B (1994) 2837–2845.
15. S. Kumar & C. E. Brennen, Some nonlinear interactive effects in bubbly clouds, *J. Fluid Mech.* **253** (1993) 565–591.
16. W. Lauterborn, Numerical investigation of nonlinear oscillations of gas bubbles in liquids, *J. Acoust. Soc. Am.* **59**(2) (1976) 283–293.
17. L. G. Leal, *Laminar Flow and Convective Transport Processes* (Butterworth-Heinemann, Boston, 1992).
18. H. Maekawa & N. N. Mansour, Control of structures and time-averaged flow properties of a plane wake by subharmonic instability modes, *J.S.M.E. Int. J. Ser. B* **37**(4) (1994) 806–814.
19. E. Ott, C. Grebogi, & J. A. Yorke, Controlling chaos, *Phys. Rev. Lett.* **64**(11) (1990) 1196–1199.
20. J. Pan, S. D. Snyder, C. H. Hansen, & C. R. Fuller, Active control of far-field sound radiated by a rectangular panel—A general analysis, *J. Acoust. Soc. Am.* **91**(4) Pt. 1 (1993) 2056–2066.
21. U. Parlitz, V. Englisch, C. Scheffczyk, & W. Lauterborn, Bifurcation structure of bubble

- oscillators, *J. Acoust. Soc. Am.* **88**(2) (1990) 1061–1077.
22. A. Prosperetti, N. Q. Lu, & H. S. Kim, Active and passive acoustic behavior of bubble clouds at the ocean's surface, *J. Acoust. Soc. Am.* **93**(6) (1993) 3117–3127.
  23. J. A. Rooney, Other nonlinear acoustic phenomena, in *Ultrasound: Its Chemical, Physical and Biological Effects*, ed. by K. S. Suslick (VCH Publishers, New York, 1988).
  24. K. Sarkar & A. Prosperetti, Backscattering of underwater noise by bubble clouds, *J. Acoust. Soc. Am.* **93**(6) (1993) 3128–3138.
  25. T. Shinbrot, Progress in the control of chaos, *Adv. Phys.* **44**(2) (1995) 73–111.
  26. H. Svensmark, J. Bindslev Hansen, & N. Pedersen, Influence of noise and near-resonant perturbations on bifurcations in Josephson junctions, *Phys. Rev. A* **35**(3) (1987) 1457–1459.
  27. H. Svensmark & M. R. Samuelsen, Influence of perturbations on period-doubling, *Phys. Rev. A* **36**(5) (1987) 2413–2417.
  28. H. Svensmark & M. R. Samuelsen, Perturbed period-doubling bifurcation. I. Theory, *Phys. Rev. B* **41**(7) (1990) 4181–4188.
  29. A. J. Szeri, Exploitation of Brownian motions for the optimal control of fiber orientation distributions, *Phys. Fluids* **8**(6) (1996) 1384–1388.
  30. S. T. Vohra, L. Fabiny, & K. Wiesenfeld, Observation of induced subcritical bifurcation by near-resonant perturbations, *Phys. Rev. Lett.* **72**(9) (1994) 1333–1336.
  31. S. T. Vohra & K. Wiesenfeld, Experimental test of the normal form for period-doubling bifurcations, *Physica D* **86** (1995) 27–33.
  32. H. O. Wang & E. H. Abed, Bifurcation control of a chaotic system, *Automatica* **31**(9) (1995) 1213–1226.
  33. C. Wargitsch & A. Hübler, Resonances of nonlinear oscillators, *Phys. Rev. E* **51**(2) (1995) 1508–1519.
  34. K. Wiesenfeld & B. McNamara, Period-doubling systems as small-signal amplifiers, *Phys. Rev. Lett.* **55**(1) (1985) 13–16.
  35. K. Wiesenfeld & B. McNamara, Small-signal amplification in bifurcating dynamical systems, *Phys. Rev. A* **33**(1) (1986) 629–642.
  36. S. W. Yoon, L. A. Crum, A. Prosperetti, & N. Q. Lu, An investigation of the collective oscillations of a bubble cloud, *J. Acoust. Soc. Am.* **89**(2) (1991) 700–706.
  37. P. K. Yuen & H. H. Bau, Rendering a subcritical Hopf bifurcation supercritical, *J. Fluid Mech.* **317** (1996) 91–109.